Supplement of

The pulsating nature of large-scale Saharan dust transport as a result of interplays between mid-latitude Rossby waves and the North African Dipole Intensity

E. Cuevas[1], A. J. Gómez-Peláez[1], S. Rodríguez[1], E. Terradellas[2], S. Basart[3], R. D. García[1,4], O. E. García[1], and S. Alonso-Pérez[5]

[1]Izaña Atmospheric Research Centre (AEMET), c/ La Marina, 20, 38001 Santa Cruz de Tenerife, Spain

[2]SDS-WAS Regional Centre (AEMET), Edificio Nexus II, c/ Jordi Girona, 29, 08034 Barcelona, Spain

[3]Earth Sciences Department, Barcelona Supercomputing Centre, Edificio Nexus II, c/ Jordi Girona, 29, 08034 Barcelona, Spain

[4]Air Liquide S.A., Delegación de Canarias, Plaza Industrial Valle Güímar Manz, 38500 Güímar, Santa Cruz de Tenerife, Spain

[5]Universidad Europea de Canarias, Campus de la Orotava, c/ Inocencio García 1, 38300 La Orotava, Santa Cruz de Tenerife, Spain

Corresponding author: E. Cuevas (ecuevasa@aemet.es), tel.: +34922151718

S1. Wind anomaly at 700 hPa for summer months with negative and positive NAFDI, in the period 2003-2012.

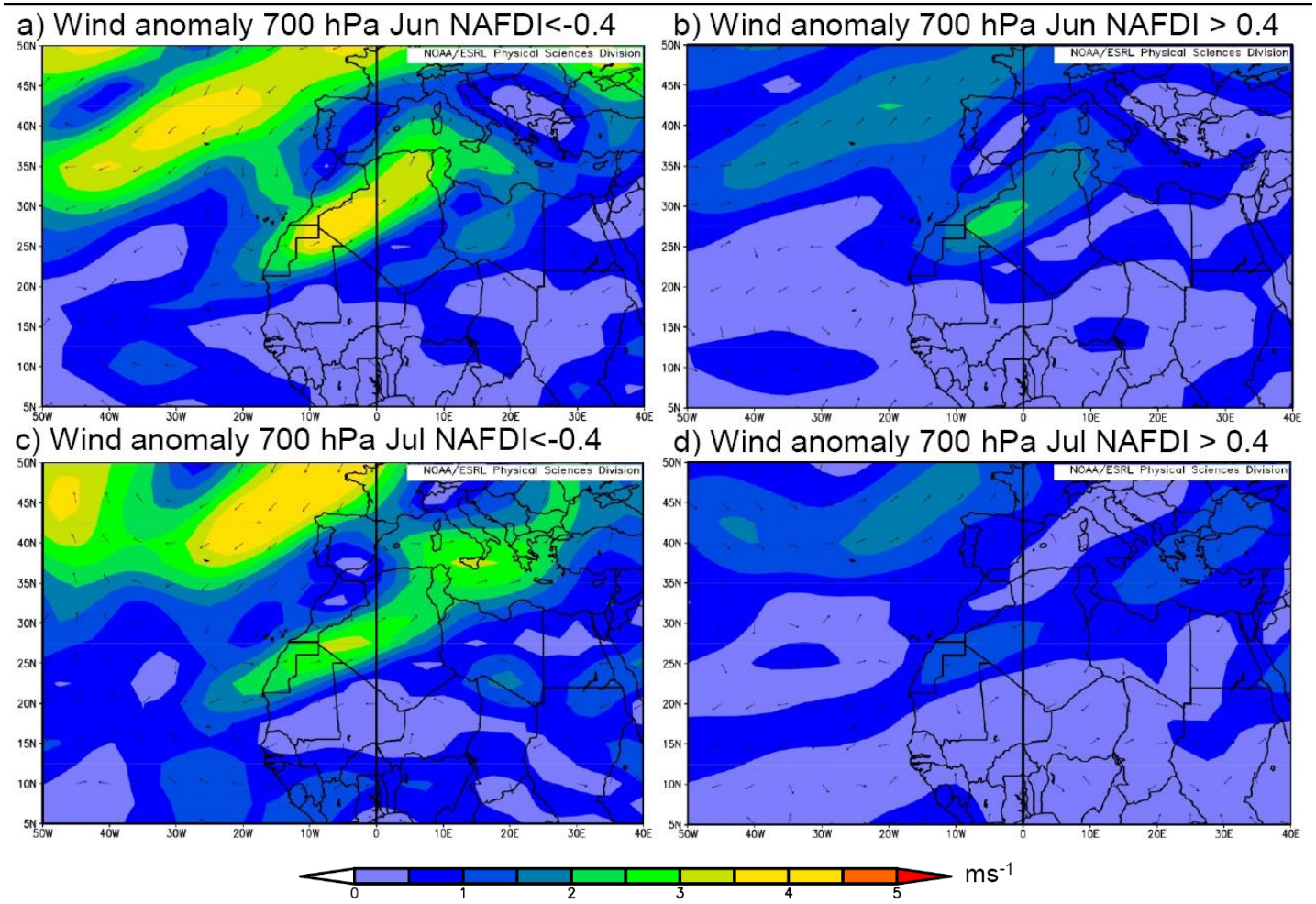

Figure S1a. Monthly anomalies of NCEP/NCAR wind vector and speed at 700 hPa for June and, July for negative (a and c) and positive (b and d,) NAFDI phases in the period 2003-2012.

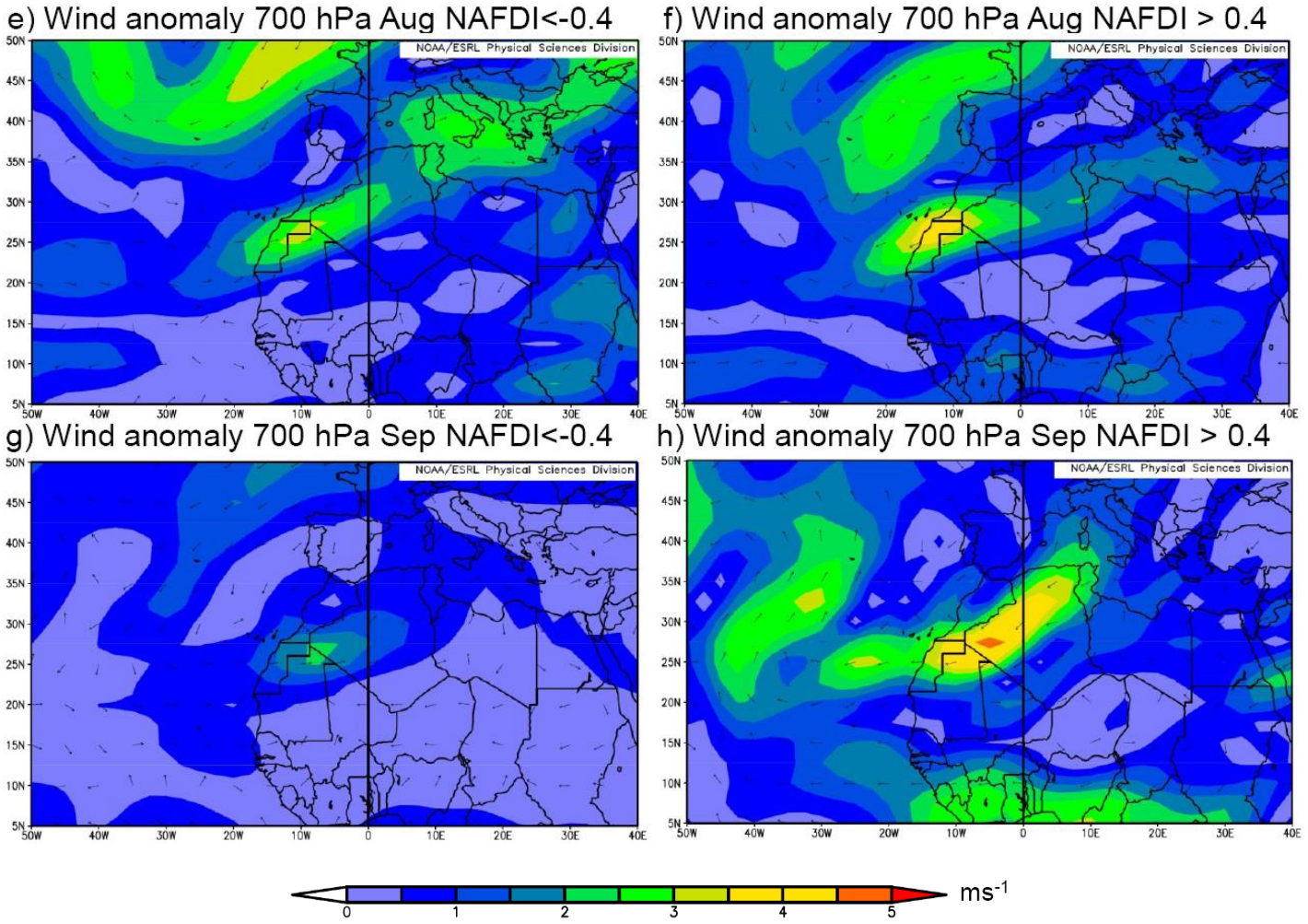

Figure S1b. Monthly anomalies of NCEP/NCAR wind vector and speed at 700 hPa for August and September, for negative (e and g) and positive (f and h) NAFDI phases in the period 2003-2012.

S2. Averaged AOD anomalies from MACC in summer for negative and positive NAFDI.

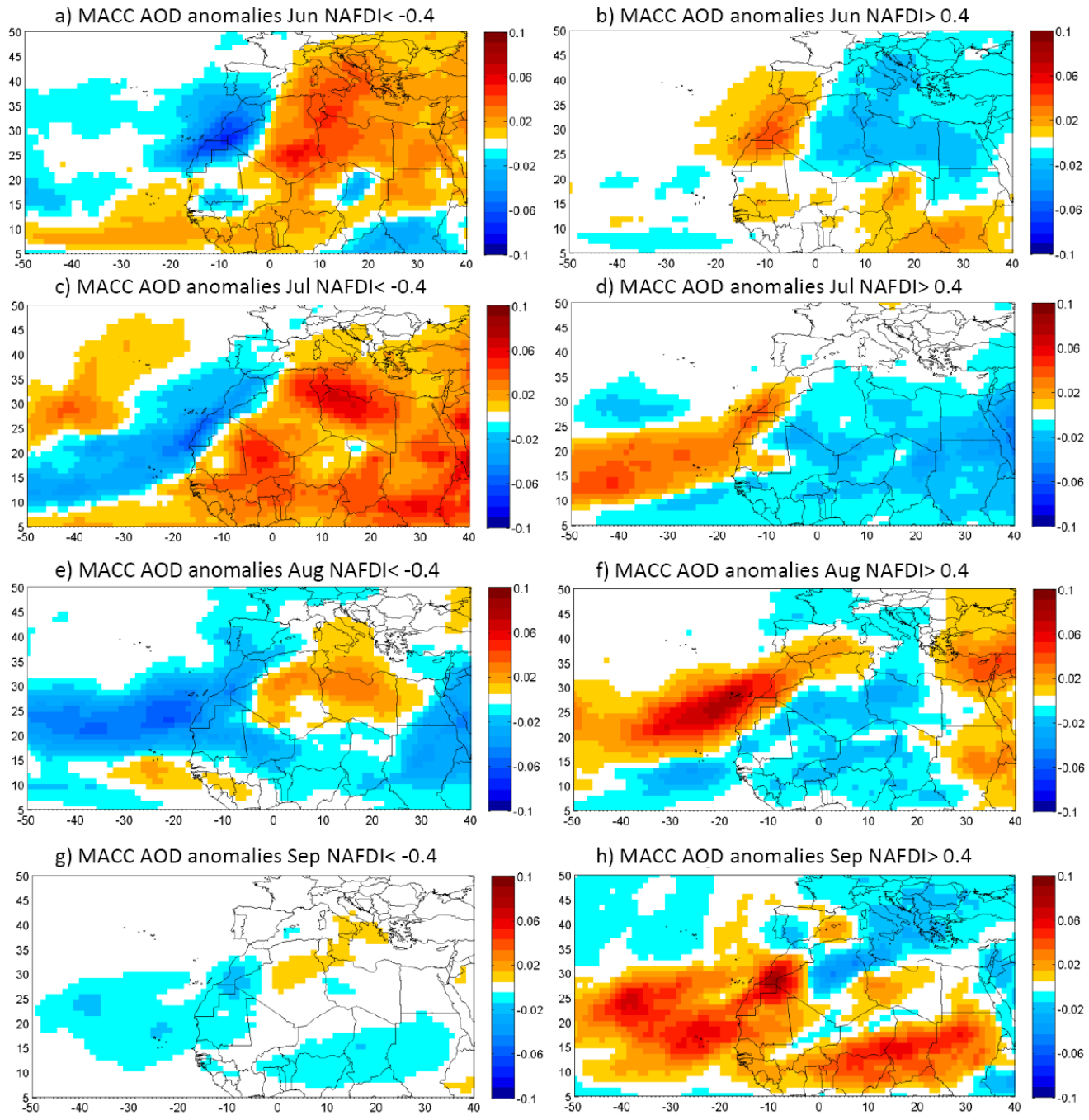

Figure S2. Averaged AOD anomalies from MACC reanalysis for summer months (June, July, August, and September) with negative (a, c, e, and g) and positive (b, d, f, and h) NAFDI phases, in the period 2003-2012. These plots were obtained by averaging the AOD anomalies for each month and each phase of the NAFDI.

S3. Monthly correlation plots between NAFDI and 200, 500, 700, 850 and 1000 hPa geopotential height in July and August, for the period 1980-2013.

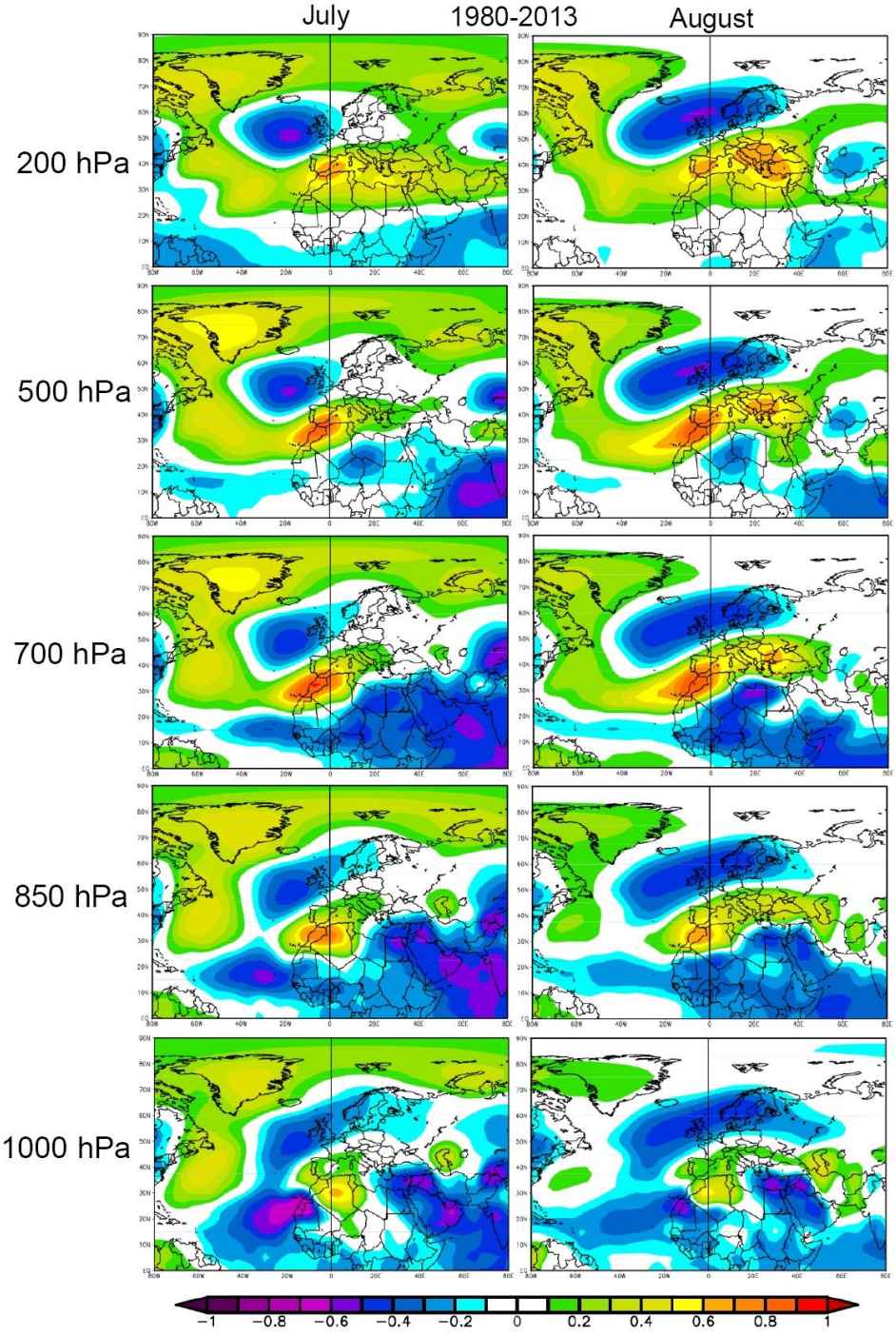

Figure S3. NCEP monthly correlation plots between NAFDI and 200, 500, 700, 850 and 1000 hPa geopotential height fields in July (left column) and August (right column), for the period 1980-2013. Correlations greater (in absolute value) than 0.34 are significant with a 95% confidence level.

S4. Wind vector and speed at 925 hPa for summer months (June, July, August, and September) with positive and negative NAFDI phases, in the period 2003-2012.

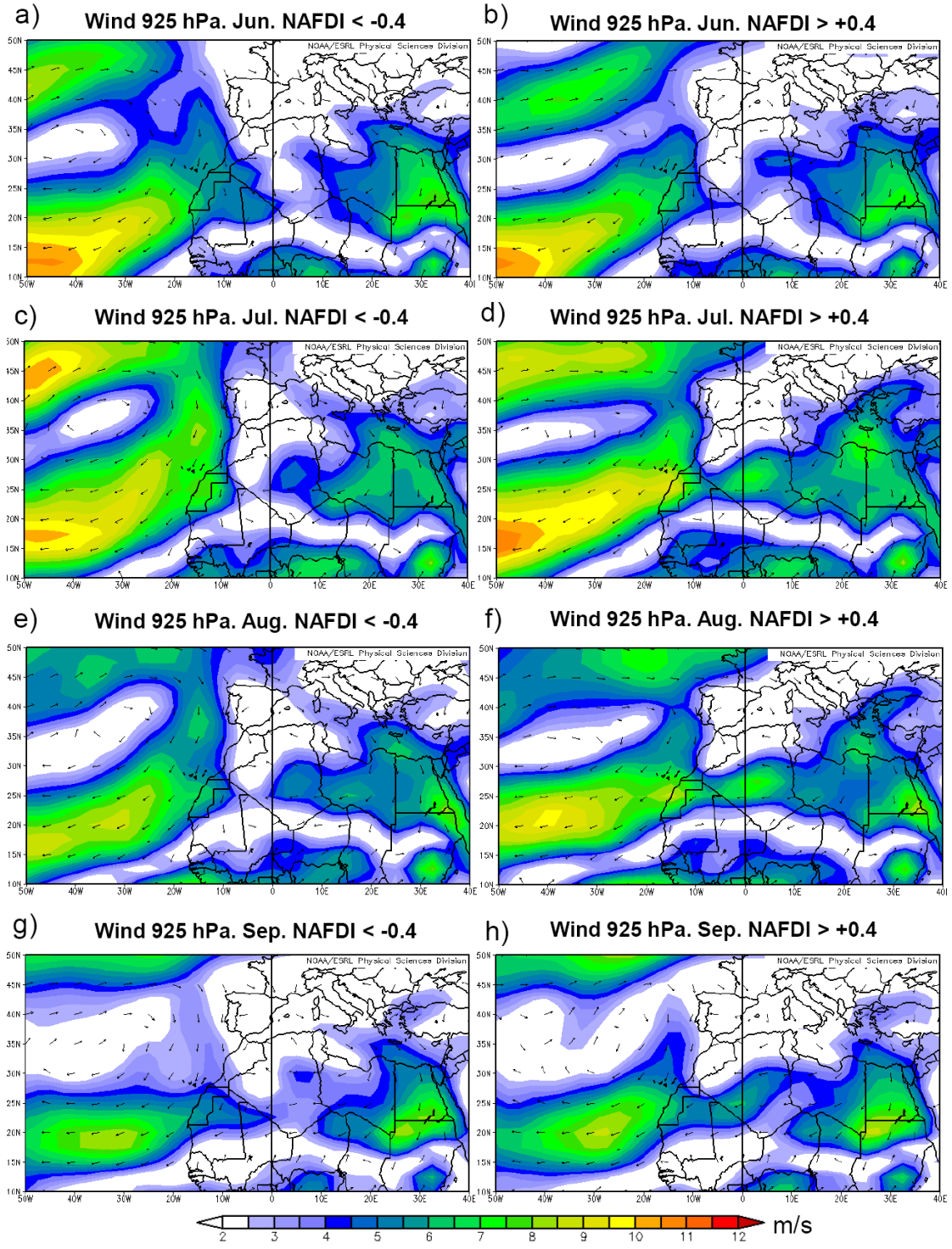

Figure S4. Monthly averages of NCEP/NCAR wind vector and speed at 925 hPa for summer months (June, July, August, and September) with negative (a, c, e, and g) and positive (b, d, f and h) NAFDI phases, in the period 2003-2012.

S5. Convective boundary layer (CBL) height (m) anomalies for summer months

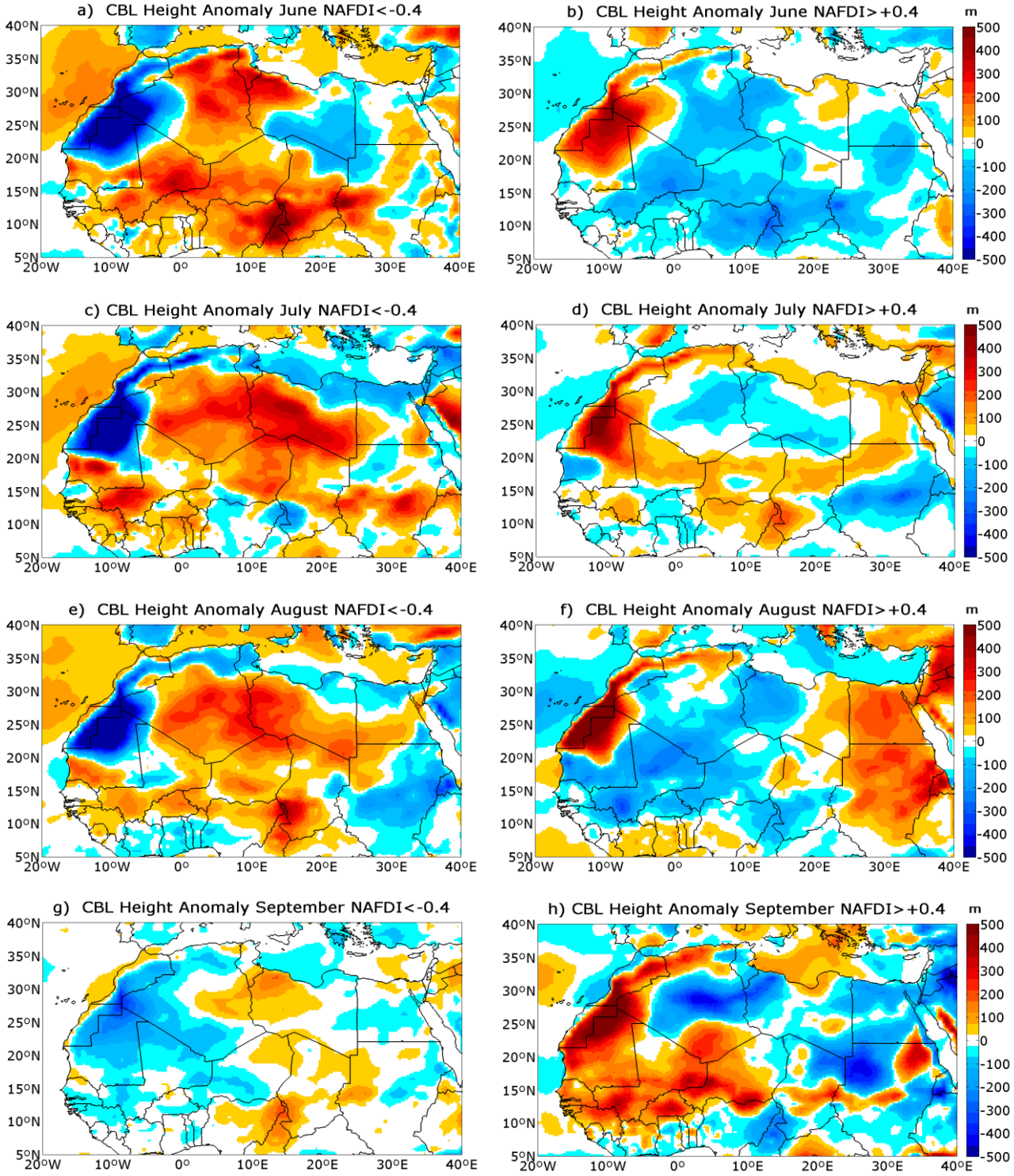

Figure S5. Monthly averages of ECMWF convective boundary layer (CBL) height (m) anomalies for summer months (June, July, August, and September) with negative (a, c, e, and g) and positive (b, d, f, and h) NAFDI phases, in the period 2003-2012.

S6. Some remarks concerning the computation of statistical confidence levels for the Pearson correlation coefficient

For the computation of statistical confidence levels for the Pearson correlation coefficient in the paper, we use tabulated values of "critical values for Pearson's correlation coefficient" for a two-tailed (or non-directional) test. As stated in the main paper, for the spatial monthly correlation plots of the period 1980-2013 (i.e., 34 years), the critical value for having a significant Pearson´s correlation coefficient with a 95% confidence level is 0.34, when using only one month per year (e.g., August). We keep the same critical value when using more than one summer month per year, considering it as an upper bound to the real one, since there might be no null auto-correlation between the months of the same year.

To assess the level of confidence about the fact that one Pearson correlation coefficient (r_2) is significantly larger than another one (r_1) we proceed as follows (e.g., Meko, 2015): 1) apply a Fisher transformation from the variables r to z, and compute the standard error of z; 2) compute the difference D between z_2 and z_1, the standard error of such difference, and standardise the difference (i.e., compute the ratio between D and its standard error); 3) apply a one-tailed (or directional) test to the standardised D using the standard normal distribution function, to obtain the confidence level about the fact that r_2 is larger than r_1.

S6.1 Method used for daily time series with time-lag autocorrelation

Assuming that there is no time-lag autocorrelation in any of the daily time series (NAFDI, SHLLSI, WA300 and OM500), the critical value for having a significant Pearson´s correlation coefficient (R) with a 95% confidence level is 0.036 (i.e., the correlation is significant if $|R|>0.036$).

However, indeed, there is time-lag autocorrelation in the daily time series. We have used the method exposed here to establish an upper bound for the critical value of the Pearson's correlation coefficient. In the four time series (NAFDI, SHLLSI, OM500 and WA300) the autocorrelation decreases when increasing the time-lag. The maximum time-lag (MTL) in which there is still a significant autocorrelation (larger than 0.036) is: 22 days for the NAFDI time series, 23 days for the SHLLSI time series, 7 days for the OM500 time series, and 15 days for the WA300 time series. Then, to establish an upper bound to the critical value, we consider a lower bound of the number of independent values (LBNIV) in the time series, computed as the ratio between 3060 (number of elements in each time series) and MTL. Note that this is a very conservative estimation of the lower bound. For correlations including the SHLLSI,

LBNIV is 133, and the upper bound to the 95%-confidence-level critical values is 0.17. For correlations including NAFDI but not including SHLLSI, LBNIV is 139, and the upper bound to the 95%-confidence-level critical values is 0.166. However, for correlations not including the former two time series but WA300, LBNIV is 204, and the upper bound to the 95%-confidence-level critical values is 0.137.

Concerning the daily time series of Sect. 3.2.2 for the terms of the energy equation, the number of elements in the time series is: 3026 when all the stages are considered, 623 when only the "driving stage" is considered, and 630 when only the "restoring stage" is considered. To compute confidence levels for the daily correlations presented in section 3.2.2, we have applied the method described in the previous paragraph but using the pertinent number of elements instead of 3060.

S7. Details concerning the numerical computations of the energy-equation terms

In Sect. 3.2.2 we use the energy equation of the atmospheric dynamics and the NCEP/NCAR reanalysis to prove that NAFDI drives SHLLSI. In this supplement we provide some details on how the numerical computations have been carried out.

We use the NCEP/NCAR reanalysis with the highest time resolution available (6-hourly, with data at 00, 06, 12 and 18 UTC, hereafter called main hours). We denote the time resolution of the reanalysis as Δt (=0.25 days), and its spatial resolution as Δx and Δy, for the longitudinal and latitudinal direction, respectively, associated to the 2.5º NCEP/NCAR grid resolution (note that the lengths of Δx and Δy depend on latitude).

To compute the different terms of Eq. (3), we proceeded as follows. For computing the time derivative, we have used a centred difference scheme (e.g, see Morton & Mayers, 1994) with total step Δt centred at the hours 03, 09, 15, and 21 UTC, hereafter called intermediate hours (e.g., for computing the time derivative at 03 UTC, we have used the temperature at 00 and 06 UTC). For computing the horizontal advection, we have proceeded in two steps: 1) computation of the advection at the main hours using a centred difference scheme with total step $2\Delta x$ in the longitudinal direction and $2\Delta y$ in the latitudinal direction, and 2) computation of the advection at the intermediate hours as the mean of the advections corresponding to the immediately previous and posterior main hours. For computing the temperature tendency due to omega at the 925, 850, and 700 hPa levels, we have proceed in two steps: 1) computation of the pressure

derivative at the main hours using a centred difference scheme that uses the potential temperature at the immediately above and below pressure levels (e.g., the levels 925 and 700 hPa for computing the vertical quasi-advection at the level 850 hPa), and 2) computation of the temperature tendency due to omega at the intermediate hours as the mean of the values corresponding to the immediately previous and posterior main hours. Note that since we are not solving a partial differential equation (the solution is already known for every time step, since it is provided by the NCEP/NCAR reanalysis), we do not need to worry about the stability of the numerical integration schemes. Finally, we have computed the diabatic heating at the intermediate hours as the residual of Eq. (3).

Once all the terms of Eq. (3) were computed at the intermediate hours (6-hourly time resolution), we proceeded as follows to compute daily values for the terms of Eq. (4). We used daily values of SHLLSI to compute its time derivative as a centred difference with total step 1 day centred at the hour 00 UTC. In this same way, the last term on the right-hand side of Eq. (4) was computed. Note that the following equation relating the numerical 6-hourly time derivatives with the daily one, holds:

$$\frac{\partial T^{n+1,n}}{\partial t} = \frac{1}{16}\left(\frac{\partial T^{n+1}}{\partial t}_{15} + 2\frac{\partial T^{n+1}}{\partial t}_{9} + 3\frac{\partial T^{n+1}}{\partial t}_{3} + 4\frac{\partial T^{n}}{\partial t}_{21} + 3\frac{\partial T^{n}}{\partial t}_{15} + 2\frac{\partial T^{n}}{\partial t}_{9} + \frac{\partial T^{n}}{\partial t}_{3}\right) \qquad (S1),$$

where the term on the left-hand side is the centred-difference time derivative between days n+1 and n, and the terms on the right-hand side are 6-hourly centred-difference time derivatives centred at the hour indicated in the sub-index corresponding to the day indicated in the super-index. Therefore, to compute *HAdv*, *Ome* and *Diab* we have proceeded in two steps: 1) computation of *HAdv* and *Ome* at the intermediate hours using Eqs. (5) and (6) and the 6-hourly terms previously computed for Eq. (3), 2) computation of the daily values centred at 00 UTC using the corresponding equation completely equivalent to (S1). In order to be consistent, to compute correlations with terms of Eq. (4), we have used SHLLSI and NAFDIDI centred at 00 UTC, as the mean of the immediately previous and posterior day.

S8. Analytical relations, equation that describes the Omega field associated to the Rossby wave in terms of the Geisler and Dickinson (1975) eigenvector, and empirical relation with the vertical shear of the zonal flow

Geisler and Dickinson (1975) obtained solutions for external Rossby modes on a beta-plane with realistic vertical wind shear, $u_0(p)$. They assume an atmosphere isothermal in the vertical

direction but with a latitude-dependent temperature, $T_0(y)$. They use the log pressure coordinate $z=ln(p_r/p)$, where p_r is a reference pressure at the ground. However, for easiness of presentation here, we are going to use the pressure as vertical coordinate except for the function $\psi(z)$ that is introduced latter. They consider small perturbations to the background flow in the form (we use geopotential instead of geopotential height):

$$\Phi'(x,y,z,t) = f_0\left(\frac{p_r}{p}\right)^{1/2}\psi(z)\exp\left[i\left(kx+ly-kct\right)\right] \quad \text{(S2)},$$

where the left hand side is the perturbed geopotential, f_0 is the Coriolis parameter at a reference latitude, k is the longitudinal wavenumber, l is the latitudinal wavenumber, and kc is the Eulerian angular frequency (i.e., they perform Fourier analysis in the latitudinal and longitudinal coordinate as well as in time). In the absence of background zonal wind, the function $\psi(z)$ is equal to $\left(p/p_r\right)^{3/14}$. They introduce this form of the perturbed geopotential into the perturbed quasi-geostrophic potential vorticity equation (considering appropriate boundary conditions) and reduce the problem to an eigenvalue problem for the eigenvector $\psi(z)$ with a set of two ordinary differential equations in z, which they solve numerically.

From the perturbed geopotential height, all the perturbed variables can be obtained using the quasi-geostrophic relations (e.g., Holton, 1992). For example, this is the equation that holds for the perturbed zonal flow:

$$u'(x,y,z,t) = -il\left(\frac{p_r}{p}\right)^{1/2}\psi(z)\exp\left[i\left(kx+ly-kct\right)\right] \quad \text{(S3)}$$

Using the perturbed quasi-geostrophic energy equation (e.g., see Holton, 1992), we have obtained the following equation for the perturbed omega:

$$\omega'(x,y,z,t) = \frac{iR}{p\sigma(p)}\left[\left(u_0(p)k-kc\right)\frac{f_0}{R}\left(\frac{\psi(z)}{2}+\frac{\partial\psi(z)}{\partial z}\right)+k\psi(z)\frac{\partial T_0}{\partial y}\right]\left(\frac{p_r}{p}\right)^{1/2}\exp\left[i\left(kx+ly-kct\right)\right] \quad \text{(S4)},$$

where R is the gas constant for dry air,

$$\sigma(p) = -R\frac{T_0(y_0)}{p}\frac{d\ln\theta_0}{dp} \qquad \text{(S5)},$$

and θ_0 is the potential temperature of the unperturbed atmosphere.

In the case of no zonal velocity, $\psi(z)$ depends much less on z than in the case with vertically-sheared zonal wind (for the latter, see Figure 10 of Geisler and Dickinson, 1975, which corresponds to external Rossby modes; for the former see the curve denoted as "Barotropic" in Figure S8-1 of this Supplement). In the latter case (sheared flow), $\psi(z)$ has a relatively prominent maximum in the lower and middle troposphere (see also the curve denoted as "NAFDI Driver" in Figure S8-1). That is, the vertical shear of the zonal wind allows the free Rossby wave to have a very significant amplitude in the middle and lower troposphere. We expect from Eq. S4 that the perturbed omega at a given level will be very roughly proportional to the value of $\psi(z)$ at such level. Based on these results, we use in the paper the Omega at 500 hPa as a tracer of the capacity of the free barotropic Rossby wave to penetrate deep into the lower troposphere. We use the term "go deep in the lower troposphere" because in the real atmosphere we expect the free Rossby waves to transport longitudinally their energy along the upper troposphere (the lower troposphere has a less zonal flow, i.e., it has a significant contribution of the meridional flow that changes a lot in longitude) and that the Rossby wave is noticed more or less in the lower troposphere depending on the vertical shear of the zonal wind. In the next paragraph, we show numerically that this relation holds.

In order to test the relation between the amplitude of OM500 (defined in Section 3.4 of the paper) and the vertical shear of the background zonal wind, we have obtained NCEP daily zonal wind time series at 2.5°E and 32.5°N for the level 200 hPa (denoted as ZWB200). In some sense, the ZWB200 value is by itself representative of the mean vertical shear of the background zonal wind, due to the fact that the wind speed is much smaller near the ground than at 200 hPa (see Fig. S8-2). Since indeed we do not have the amplitude of OM500 but its instantaneous daily value, we compute the daily correlation using only days for which the absolute value of the NAFDIDI is greater than a threshold (we expect the instantaneous value of OM500 approaches the OM500 amplitude as the threshold grows). The correlation between the daily ZWB200 and OM500 time series for days in which the absolute value of the NAFDIDI is larger than 1.3, is 0.251; whereas if the NAFDI threshold is set at 2.6 (3.9) the correlation becomes 0.297 (0.335). These daily correlation values do not decrease significantly if a 15-day or 29-day running mean is applied previously to the ZWB200 time series.

Note that the Geisler and Dickinson (1975) background zonal flow does not have latitudinal dependence, and therefore does not account for the latitudinal waveguide phenomenon.To describe in a more accurate way the propagation of these Rossby waves in the real atmosphere, a much more sophisticated (and difficult) mathematical model would be necessary (not done in the literature according to our knowledge): a background zonal flow depending "strongly" in latitude and height, and depending "slightly" in longitude. The perturbation problem for such background flow would lead to an eigenvalue problem with Partial Differential Equations depending on latitude and height simultaneously, combined with a WKB method in the longitudinal direction and Fourier analysis in time.

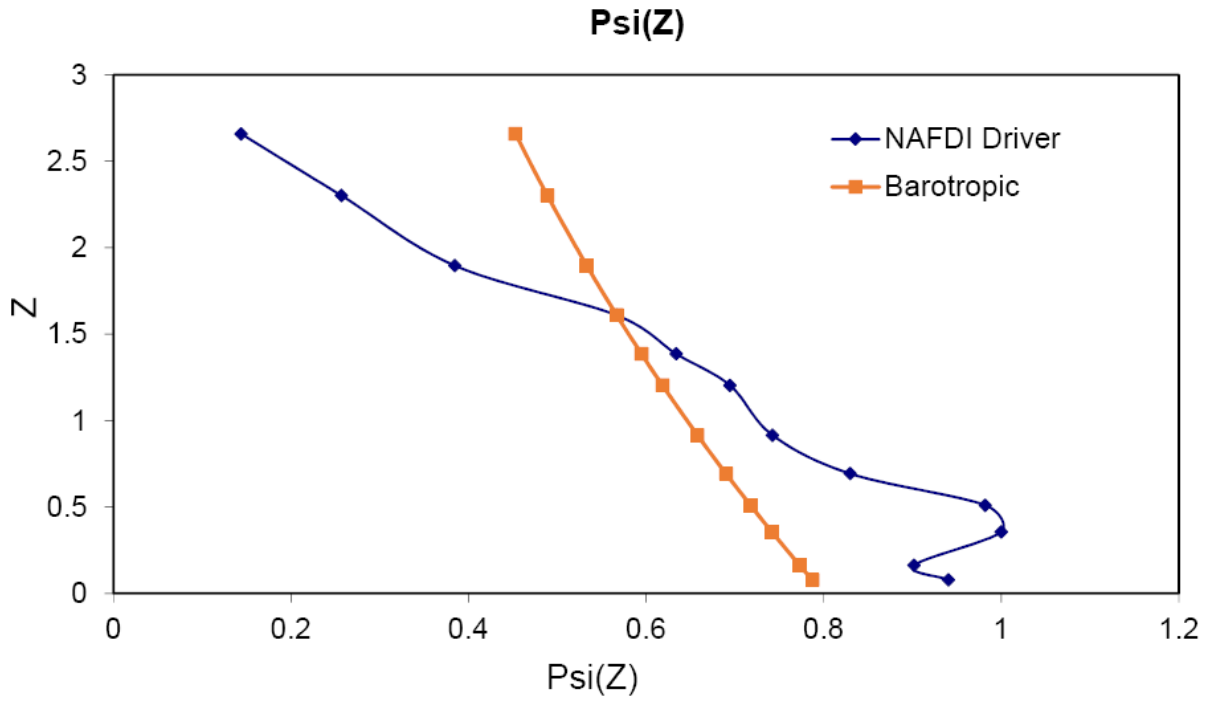

Figure S8-1. Vertical structure of the Rossby wave that drives the NAFDI variations represented using the same variables than Geisler and Dickinson (1975), for comparison (they are very similar) with the vertical structure of the external Rossby wave of Geisler and Dickinson (1975) with "effective wavenumber" 10.8 (see their Figure 10). As reference, the case with no zonal velocity (denoted "Barotropic") has been also plotted.

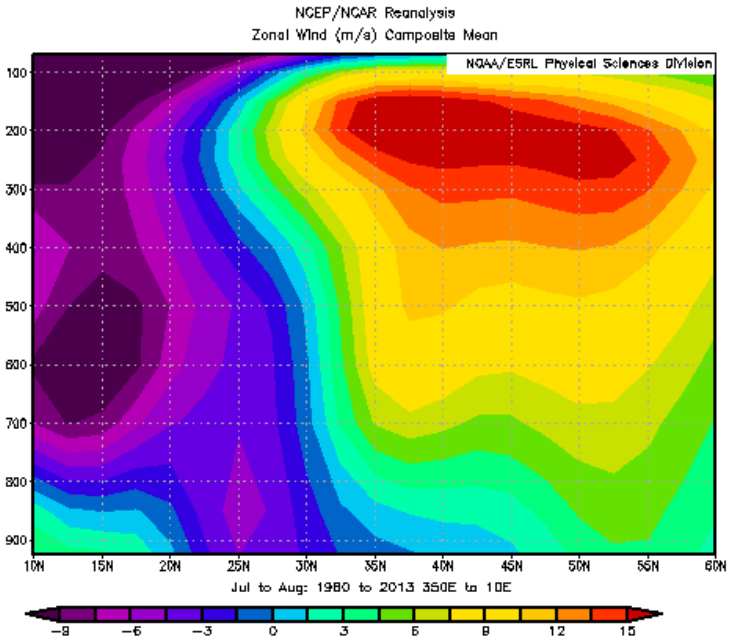

Figure S8-2. Mean zonal wind (averaged also in longitude from 10°W to 10°E) for a latitude-vertical cross-section during the period July-August 1980-2013.

S9. NCEP monthly correlation and regression maps between the monthly NAFDI and omega, for summer months in the period 1980-2013.

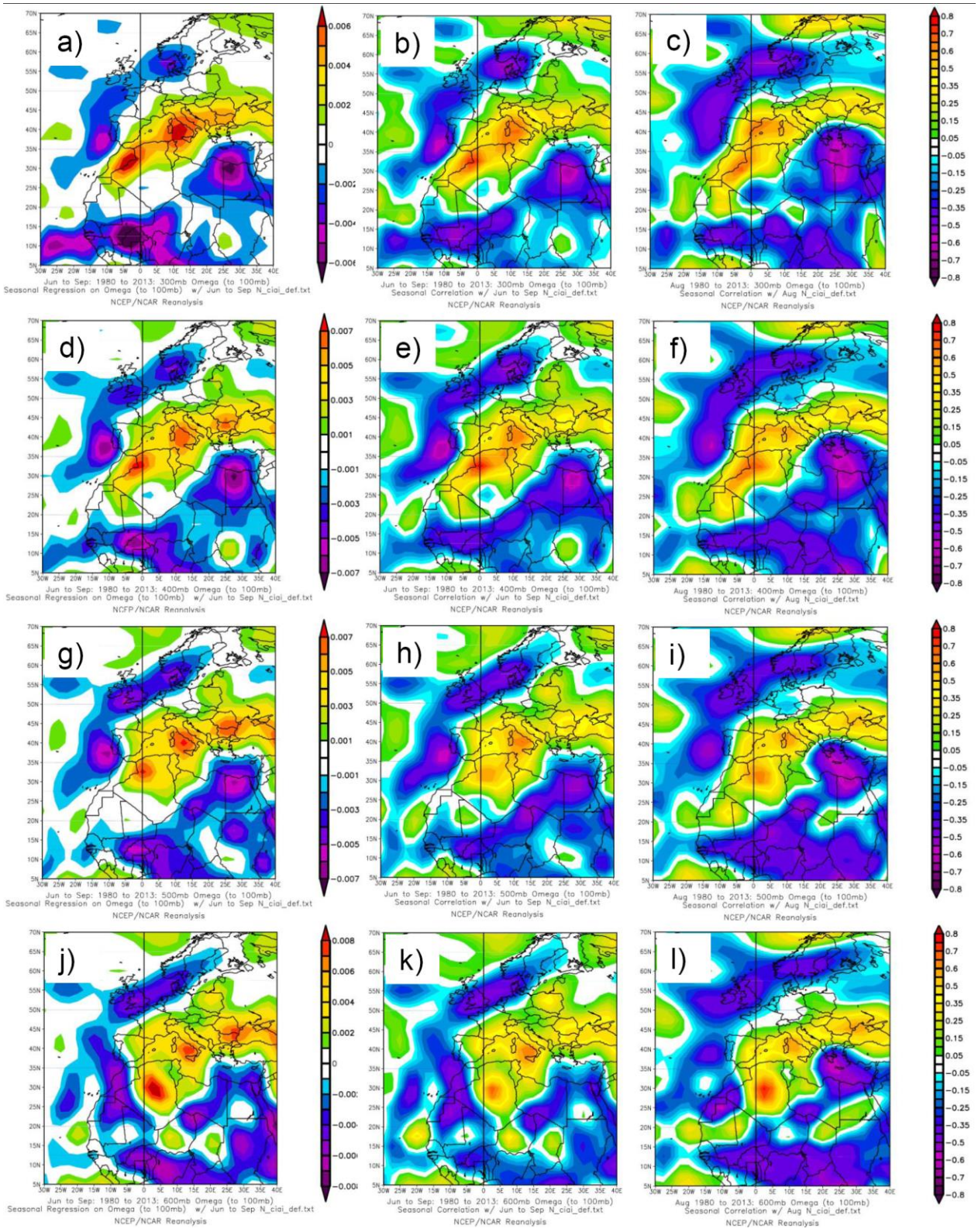

Figure S9-1. NCEP monthly regression plots (Pa/s/NAFDI) between the omega at 300, 400, 500 and 600 hPa (from top to bottom; a, d, g, j) and the monthly NAFDI for June-September

of the period 1980-2013. Correlation plots between the omega at the same pressure levels and the monthly NAFDI for June-September (b, e, h, k) and for August (c, f, i, l) of the period 1980-2013. Correlations greater (in absolute value) than 0.34 are significant with a 95% confidence level.

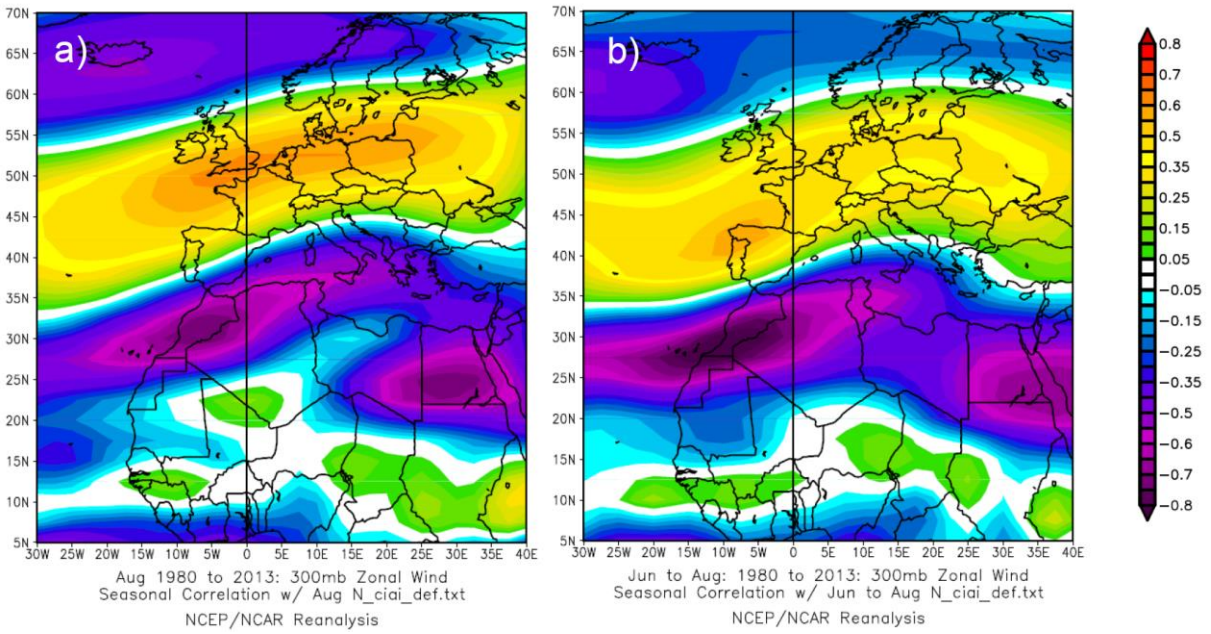

Figure S9-2. NCEP monthly correlation plots between the zonal wind at 300 hPa and the monthly NAFDI for August months (a) and for June-September (b) of the period 1980-2013. Correlations greater (in absolute value) than 0.34 are significant with a 95% confidence level.

S10. Power spectra of the time series

We have computed the power spectra of the daily NAFDIDI, SHLLSI, and LCWAOM time series for the period 20 June -17 September 1980-2013 using Fast Fourier Transform (e.g., Press et al., 1994), after padding with zeros till complete 4096 elements in each time series (i.e., the nearest larger power of 2). Then, we have reconstructed the three time series using only the Fourier components of the intermediate time-scale range (i.e., application of a band-pass filter), and computed the Pearson daily correlation between these filtered time series. The correlations are quite similar to those previously obtained for the no-filtered time series. We have also computed the Pearson correlation between the filtered OM500 and NAFDIDI time series obtaining the value 0.49, whereas the correlation is 0.43 for the no-filtered daily time series.

This rather high correlation (0.49) confirms that the influence of OM500 on NAFDI operates in the time scales of the Rossby waves.

Figure S10-1a shows the power spectra of the NAFDIDI and SHLLSI time series in the intermediate range, after applying a 5-point running mean (note that there are 273 points - discrete Fourier frequencies- in the considered range), whereas Fig. S10-1b shows the equivalent plot for the NAFDIDI and LCWAOM time series. The total power of the full spectrum for the SHLLSI, and LCWAOM time series has been normalized to that of the NAFDIDI time series, before plotting the power spectra in Fig. S10-1 for easiness in the comparison.

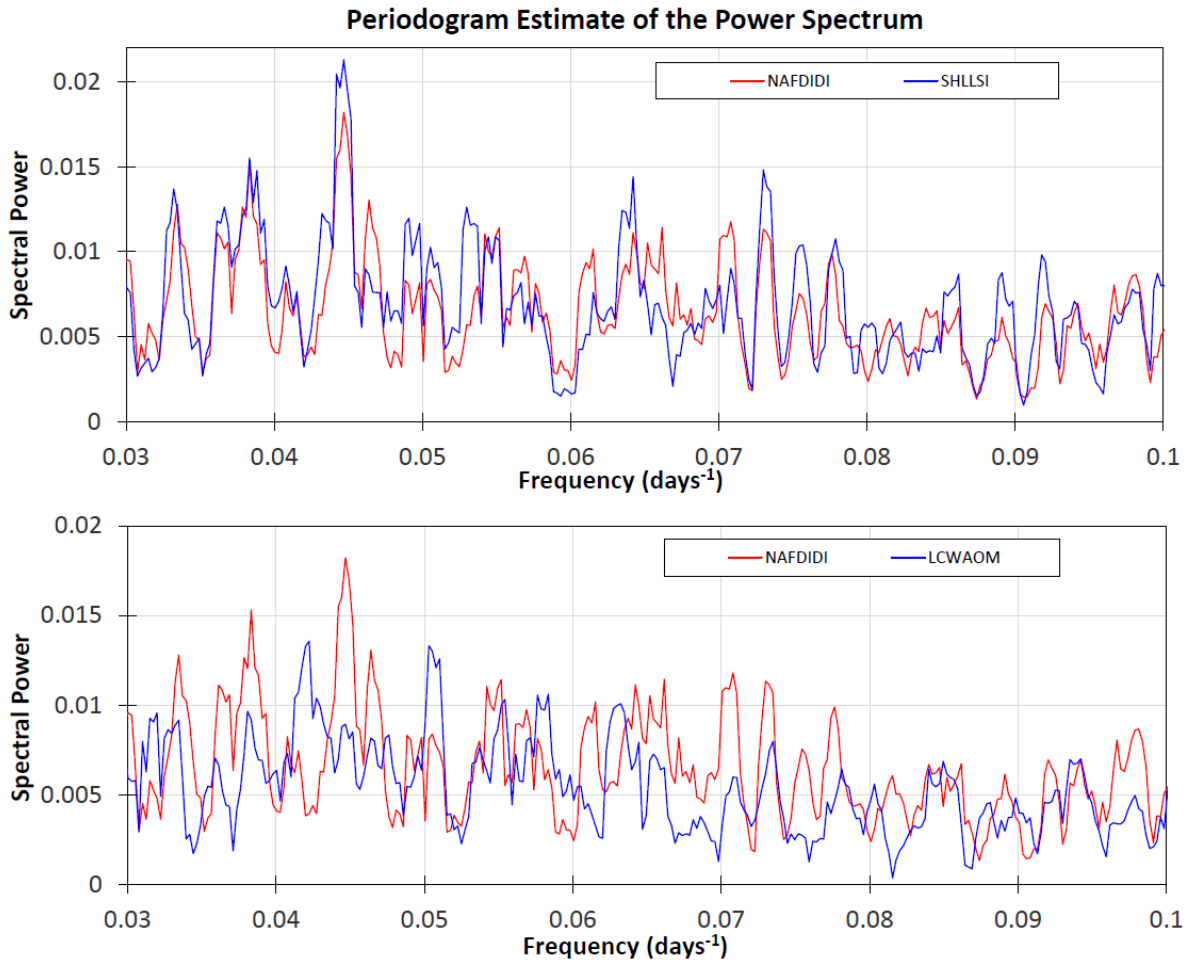

Figure S10-1. a) Upper graph: power spectra of the NAFDIDI and SHLLSI time series in the intermediate time-scale range, after applying a 5-point running mean; b) Lower graph: power spectra of the NAFDIDI and LCWAOM time series under the same conditions than in graph a).

Acknowledgements

The authors thank NCEP/NCAR Reanalysis Project at the NOAA/ESRL. All the numerical computations for Sect. 3.2.2 have been performed using the language R (R Core Team, 2016). The authors wish to thank ECMWF for providing ERA-Interim data and MACC-dust reanalysis.

References

Geisler, J. E., and Dickinson, R. E.: External Rossby modes on a beta-plane with realistic vertical wind shear, Journal of the Atmospheric Sciences, 32, 2082-2093, 1975.

Holton, J. R.: An introduction to dynamic meteorology, Third edition, International Geophysics Series, vol. 48, Academic Press, San Diego, California, 1992.

Meko, D. M., Applied Time Series Analysis, Lesson notes published on internet, GEOS 585A,Spring 2015, http://www.ltrr.arizona.edu/~dmeko/geos585a.html, 2015

Morton, K.W. and Mayers, D.F.: Numerical Solution of Partial Differential Equations, Cambridge University Press, Cambridge, 1994.

Press, W. H., Teukolsky, S. A., Vetterling, W. T., and Flannery, B. P.: Numerical Recipes in FORTRAN. The Art of Scientific Computing, Second edition reprinted with corrections, Cambridge University Press, Cambridge, 1994.

R Core Team: R: A Language and Environment for Statistical Computing, R Foundation for Statistical Computing, Vienna, Austria, https://www.R-project.org, 2016.